Early Palaeozoic intracratonic shears and post-tectonic cooling in the Rauer Group, Prydz Bay, East Antarctica constrained by ^{40}Ar/^{39}Ar thermochronology

CHRISTOPHER J.L. WILSON, CAMERON QUINN, LAIXI TONG and DAVID PHILLIPS

School of Earth Sciences, The University of Melbourne, Victoria 3010, Australia
cjlw@unimelb.edu.au

Abstract: The Rauer Group, in Prydz Bay, contains reworked Archaean-Proterozoic crust in high-strain zones that formed during a pervasive high-temperature ductile deformation event related to intracratonic mechanisms. The effects of this event extend southwards from Prydz Bay into the southern Prince Charles Mountains. The associated structural evolution involved development of ductile and brittle structures that formed during an approximately north–south directed transpressional deformation event that is confined to high-grade (>800°C) shear zones in the Rauer Group. Minerals from the Rauer Group, yield ^{40}Ar/^{39}Ar cooling ages ranging from 560 to 460 Ma. Thermal histories derived from hornblende, biotite and feldspar suggest that the onset of rapid cooling began sometime prior to 510 Ma with cooling rates of *c.* 42 to 33°C myr^{-1} from *c.* 510 Ma to *c.* 500 Ma. Whereas, ^{40}Ar/^{39}Ar data obtained from plagioclase and K–feldspar suggest a slower cooling from *c.* 500 Ma to *c.* 460 Ma with cooling rates from 5 to 2°C myr^{-1}. These results demonstrate that the early Palaeozoic cooling history and comparable palaeostress regimes are regionally extensive, which has important implications for the tectonothermal and stress-field variability across Gondwana. The elevated thermal conditions would induce lithospheric weakening and promote the early Palaeozoic intraplate orogeny observed in eastern Antarctica with the development of a large intracratonic shear system.

Introduction

The processes involved in the formation of Gondwana and the early Palaeozoic deformation in Prydz Bay and its relationship in East Antarctica has been a topic of wide interest over many years. The reconstruction of the assembly of Gondwana is, however, hampered by a lack of reliable data on the tectonothermal evolution of many of the constituent elements. This is the case in the Rauer Group where there are orogenic belts of different ages, intersecting structural trends and a late tectonothermal evolution that is rather enigmatic in the context of the final amalgamation of Gondwana (Fig. 1). East Antarctica is a central part of ancient Gondwana and is surrounded by a number of ancient accretionary zones that formed as the consequence of early Palaeozoic tectonics. These include the Mozambique suture and its extension as the Afro–Antarctic shear system, into Dronning Maud Land (Jacobs *et al.* 2003), and the Ross–Delamerian orogenic belts on the proto-Pacific margin (Fig. 1). During this time, the Precambrian sequences that make up the core of East Antarctica, in what has been referred to as the "Mawson continent" (Fanning *et al.* 1996, Fitzsimons 2000), remained reasonably unaffected by substantial mountain forming processes, although there is abundant evidence for

a thermal event at early Palaeozoic times that was accompanied by shear zone formation, simple fabrics in Neoproterozoic basins (Phillips *et al.* 2005), pegmatite and late granite intrusion throughout Prydz Bay (Carson *et al.* 1996, Zhao *et al.* 1997) and the northern Prince Charles Mountains (Boger *et al.* 2002).

Most evidence for an early Palaeozoic tectonothermal event between India and the Mawson Continent (Fig. 1) comes from the Prydz Bay region, the Rayner Complex further west, the southern Prince Charles Mountains and the syn- and post-orogenic granitoids of the Grove Mountains (Liu *et al.* 2006). In these areas the early Palaeozoic (*c.* 550–490 Ma) events have been superimposed on Archaean sequences and Neoproterozoic orogenic belts (Phillips *et al.* 2006, 2007). Within the Prince Charles Mountains the early Palaeozoic deformation manifests as fault and pegmatite emplacement (Boger *et al.* 2002, Fig. 2b1), thrusting events (Fig. 2b2) or ductile cleavages (Fig. 2b3) that can be related to obvious changes in the orientation of the stress field through time with a range of possible palaeostress orientations ranging from NW–SE and NNE–SSW (Fig. 2b3). A more northerly palaeostress orientation (Fig. 2b4) is recorded in the refolded fabrics in the Turk Glacier region
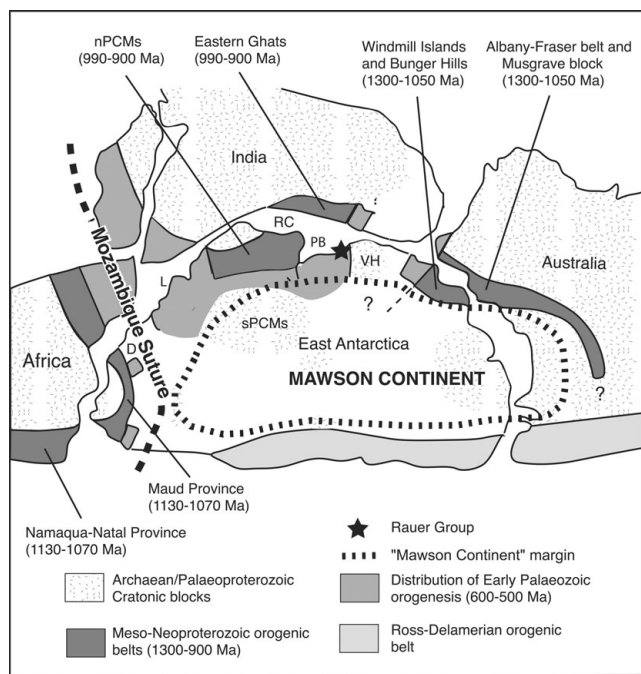
Fig. 1. Location of the study area within the margin of the 'Mawson Continent', and adjacent crustal blocks in a simplified Gondwana showing the Archaean–Palaeoproterozoic cratonic blocks, Meso–Neoproterozoic and early Palaeozoic orogenic belts (after Fitzsimons 2000). D = Dronning Maud Land, L = Lutzow–Holm Bay, nPCMs = northern Prince Charles Mountains, PB = Prydz Bay, sPCMs = southern Prince Charles Mountains, RC = Rayner Complex, VH = Vestfold Hills.

(Boger & Wilson 2005). In the Rauer Group, and much of Prydz Bay, nearly all the early Palaeozoic metamorphic assemblages, fabrics and late brittle structures are related to the highly strained portions of the basement sequence (Fig. 2c) and an approximately north to south oriented palaeostress field (Fig. 2c1).

In this contribution ^{40}Ar/^{39}Ar mineral ages from the high temperature ($>800°$C; Harley 1998, Kelsey *et al.* 2003a, Tong & Wilson 2006) granulite facies fabrics in the Rauer Group have been determined with the aim of placing constraints on the cooling history in these tectonic units. ^{40}Ar/^{39}Ar age data is provided to assess the extent of early Palaeozoic thermal overprinting on the basement rocks and to constrain the minimum age of the deformation events in the high-strain zones recognized in the Rauer Group. This new data permits tectonic correlation with the adjacent regions in southwest Prydz Bay and Prince Charles Mountains and has implications for the role of the early Palaeozoic tectonic event within the assembly of east Gondwana.

Regional geological setting

The Rauer Group are a cluster of ice free offshore islands and peninsulas located adjacent to the Archaean block of the

Vestfold Hills to the north-east, and the early Palaeozoic *c.* 515 Ma high-grade mobile belts (e.g. Brattstrand Bluff and Larsemann Hills) to the south-west in Prydz Bay (Fig. 2c1). The rocks of the Rauer Group are subdivided into: 1) Archaean orthogneiss (Kinny *et al.* 1993), which occurs mainly in north-eastern and southern parts of the region and is intruded by multiply deformed Mesoproterozoic mafic dykes (Harley & Fitzsimons 1991, Dirks *et al.* 1994), 2) a dominant Proterozoic paragneiss (Filla Paragneiss), which crops out mostly in the western and south-eastern parts of the region (Harley & Fitzsimons 1991), but was pervasively intruded by Neoproterozoic to early Palaeozoic granitic orthogneiss, and 3) the less common Mg-rich metapelite (Mather Paragneiss), which occurs as a dismembered sequence within the host enderbitic orthogneiss on Mather Peninsula (Harley & Fitzsimons 1991, Harley 1998, Sims 1999, Kelsey *et al.* 2003a). These Prydz Bay rocks and the Rayner Complex in the northern Prince Charles Mountains (Carson *et al.* 2000) represent a large region of high-grade metamorphic rocks long recognized to be part of an extensive high-grade orogenic terrane that evolved during an early Neoproterozoic (*c.* 1000 Ma) granulite facies event and a 990–900 Ma tectonothermal overprint (Fitzsimons & Thost 1992, Kinny *et al.* 1993, Carson *et al.* 2000, Fitzsimons 2000). This overprint is characterized by upper amphibolite to granulite metamorphic grades (Kinny *et al.* 1997, Boger *et al.* 2000, Carson *et al.* 2000).

Evidence of the early Palaeozoic tectonism in Prydz Bay is highly variable in scale and is preserved as discrete high-strain zones and pegmatite emplacement, distinguished through SHRIMP U–Pb dating of zircon (Kinny *et al.* 1997, Boger *et al.* 2002), or as a pervasive early Palaeozoic granulite facies tectonism (*c.* 550–465 Ma). Zhao *et al.* (1992) obtained Pb–Pb evaporation ages of 560–540 Ma for the syn-tectonic Progress Granite that were refined to 515 Ma by SHRIMP U–Pb zircon analysis (Carson *et al.* 1996). Ziemann *et al.* (2005) dated monazite from Neoproterozoic aged pegmatites that were overprinted by a 550–500 Ma granulite event. In addition garnet whole rock Sm–Nd ages of 517–467 Ma were obtained from paragneiss and leucogneiss samples (Hensen & Zhou 1995). SHRIMP U–Pb ages of 535–530 Ma for zircon and monazite in partial melt bodies (Fitzsimons 1997, Fitzsimons *et al.* 1997) in the Brattstrand Bluff region.

In the Rauer Group the extent and nature of the early Palaeozoic tectonism is controversial (Dirks & Wilson 1995, Harley & Fitzsimons 1995, Hensen & Zhou 1995, Harley *et al.* 1995). In the older Archaean and Proterozoic rocks the U–Pb zircon systematics are partially reset at 550–490 Ma (Kinny *et al.* 1993) and units are separated by localized high-strain zones, such as the Mather high-strain zone (Fig. 3), which contains early Palaeozoic ages (e.g. Hensen & Zhou 1995, Sims 1999, Kelsey *et al.* 2003b). The high-strain zones in the Rauer Group are
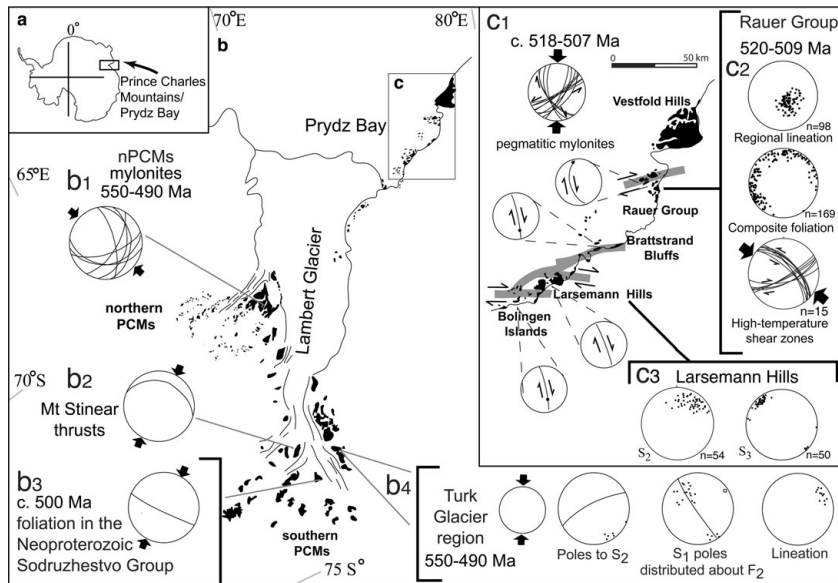
Fig. 2. Locations within the Prydz Bay Prince Charles Mountains (PCMs) region and a summary of early Palaeozoic structural features. **a.** Location in Antarctica. **b.** Maps showing distribution of structural elements and palaeostress orientations, **b1.** summary of data in Boger *et al.* 2002 that shows mylonites that accompany pegmatite emplacement, **b2.** geometry of late thrusts identified by Phillips *et al.* 2005, **b3.** orientation of foliation in the Neoproterozoic Sodruzhestvo sediments, **b4.** redistribution of earlier foliations related to a north–south shortening event. **c.** Distribution of intracratonic dextral transcurrent shear systems exposed between the Rauer Group and Larsemann Hills. The equal-area stereographic nets summarize the average orientation of early Palaeozoic features and thick black arrows give inferred compression directions. Data sources: Rauer Group Sims *et al.* 1994 and this study, Larsemann Hills Carson *et al.* 1995, Dirks & Wilson 1995, PCM data from (Boger *et al.* 2001, 2002, Boger & Wilson 2005, Phillips *et al.* 2005).

associated with the transposition and reorientation of pre-existing Neoproterozoic and older fabrics and magmatic intrusions into a single high-grade foliation that is preserved as laminar domains (Fig. 2c2). The foliation incorporates and is defined by boudinaged mafic dykes, rootless folds in mafic dykes with earlier foliations and a gneissic foliation (Sims & Wilson 1997). Throughout the Rauer Group, fold hinges converge towards an orientation that is consistently $5-10°$ shallower than a pervasive south-easterly plunging mineral lineation (mean plunge *c.* $65°$) but the populations coalesce with increasing strain (Harley 1987). In low-strain zones, the mineral lineation converges from shallowly plunging to steeply plunging with increasing strain.

Repeated deflection of the composite foliation (S_n in Fig. 3) occurred about the lineation and can be resolved into a conjugate shear system composed of complex shear zones (Figs 2c1 & 3a). The major shear structure in the Rauer Group is an east–west oriented, southerly-dipping, 3 km wide, dextral shear zone with subordinate, near orthogonal (hence conjugate), $1-3$ m wide, sinistral shear zones oriented approximately NW–SE. The geometry of the conjugate system suggests that there was a significant component of lateral, transcurrent flow, with the lineation and fold hinges perhaps tracking the maximum stretching axis of the coaxial component of flow (e.g. Jiang & Williams 1998), which implies transpressional flow (cf. Jiang *et al.* 2001) responding to north-westerly directed compression (Fig. 3a). Overprinting these are north–south trending dextral shears that contain pegmatite dykes (Sims *et al.* 1994) dated at *c.* 500 Ma (Sims 1999). The data

presented by Sims *et al.* (1994) are consistent with compression related to a palaeostress associated with a flat-lying σ_1 oriented north–south.

Elsewhere along the Prydz Bay coast at Brattstand Bluffs, Larsemann Hills and in the Bolingen Islands, east–west trending zones of high-strain have been recognized (Dirks & Wilson 1995, Dirks & Hand 1995). Two overprinting episodes of high-strain are recognized in the Larsemann Hills (Fig. 2c3) as a sequence of highly deformed rocks in a $0.5-1$ km wide dextral transpression zone (Carson *et al.* 1995) and as a series of $1-3$ km wide zones that were synchronous with the intrusion of the Progress Granite at *c.* 515 Ma (SHRIMP U–Pb age, Carson *et al.* 1996). If it is assumed that the Prydz Bay shear system correlates with the Amery Lineament (Golynsky *et al.* 2002), an east west trending linear magnetic anomaly that transects southern Prydz Bay, then continuation of the overall shear zone system can be implied over a distance of *c.* 1000 km on an east–west trajectory.

High-temperature (*c.* $950-1050°C$, $10-12$ kbar, Harley 1998, Kelsey *et al.* 2003b) sapphirine-bearing metamorphic assemblages are preserved in the high-strain zones of the Rauer Group and are overprinted by retrograde biotite+cordierite-bearing assemblages that Kelsey *et al.* (2003b) attribute to early Palaeozoic orogenesis (*c.* 511 Ma). The retrograde assemblages indicate decompression to *c.* 8 kbar and cooling to *c.* $820°C$ (Kelsey *et al.* 2003a, Tong & Wilson 2006). The tectonic setting of these high-grade highly strained rocks is pervasive tectonic reworking that has been attributed to either 1) a large-scale early Palaeozoic suture related to
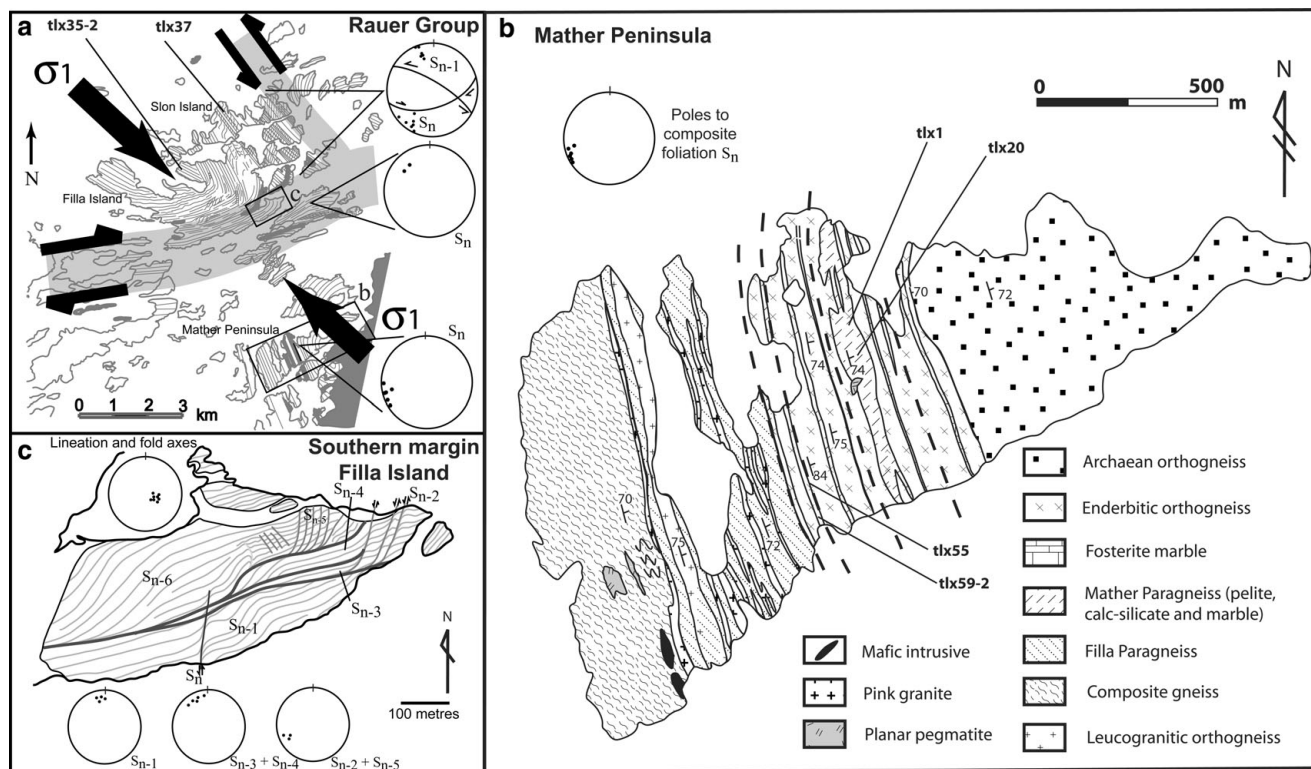
Fig. 3. Simplified geological maps and location of samples in the Rauer Group shear system that overprints and reorients Neoproterozoic structures and intrusive bodies. **a.** The overall conjugate geometry of the shear system, the equal-area stereographic nets summarize the average orientation of poles to the composite foliation that are distributed about a consistent regional lineation. The conjugate geometry implies primary transcurrent shearing with a component of tension responding to NW−SE directed compression. **b.** Lithological distribution and sample localities in the laminar fabrics of Mather Peninsula. The enderbitic orthogneisses represent a high-strain zone and the dashed lines show some cm- to m-wide high-grade shear zones. **c.** Illustrates the complex laminar fabric distribution along the southern margin of Filla Island. Seven generations of fabric (donated S_{n-6} to S_n for some value of n that represents the pre-existing fabrics) that is progressively deflected about a parallel and constant axis with the deflection implying an overall dextral shearing.

Table I. Summary of $^{40}Ar/^{39}Ar$ analysis results. Analysed minerals: hornblende, biotite and feldspar.

Lithology	Sample no.	Sites	Mineralogy	Mineral analysed	Amount analysed	TFA (Ma) ±1 SD	WMA (Ma) ±1 SD	Min. age (Ma) ±1 SD	Max. age (Ma) ±1 SD
Mafic granulite	tlx1	MP	grt-cpx-opx-hb-pl-bt-qtz	hb	8.57 mg	505.1±1.6	500.3±3.3	498.0±1.1	514.6±2.0
				bt	0.54 mg	499.1±2.0	497.9±2.5	494.9±2.3	572.2±4.7
				pl	6.60 mg	512.4±5.5	464.0±3.3	458.0±5.7	631.4±10.2
Mafic sheared	tlx55	MP	grt-cpx-opx-hb-pl-qtz	hb	6.95 mg	583.5±2.4	563.3±7.7	501.2±1.8	598.7±1.9
Leucosome	tlx20	MP	spr-opx-ksp-bt-sil-crd-pl	bt	0.52 mg	500.0±1.9	498.6±2.1	495.3±1.7	509.8±2.9
				ksp	0.53 mg	490.2±11.1	477.3±3.7	370.8±4.0	695.9±16.5
Granitic orthogneiss	tlx29	FI	grt-ksp-pl-bt-qtz	bt	0.45 mg	499.0±1.8	494.0±5.0	492.0±1.2	522.7±4.0
Granitic orthogneiss	tlx35-2	FI	grt-bt-ksp-pl-qtz	bt	0.72 mg	499.2±2.4	500.6±1.7	236.7±3.8	643.1±18.8
Granitic orthogneiss	tlx37	SI	ksp-pl-qtz ± grt ±bt	ksp	0.64 mg	495.4±2.1	508.7±8.5	333.0±9.9	561.5±9.8

Abbreviations: MP = Mather Peninsula, FI = Filla Island, SI = Slon Island, grt = garnet, cpx = clinopyroxene, hb = hornblende, opx = orthopyroxene, bt = biotite, pl = plagioclase, ksp = K-feldspar, spr = sapphirine, crd = cordierite, spl = spinel, sil = sillimanite, qtz = quartz, TFA = Total fusion age, WMA = weighted mean age, SD = standard deviation.
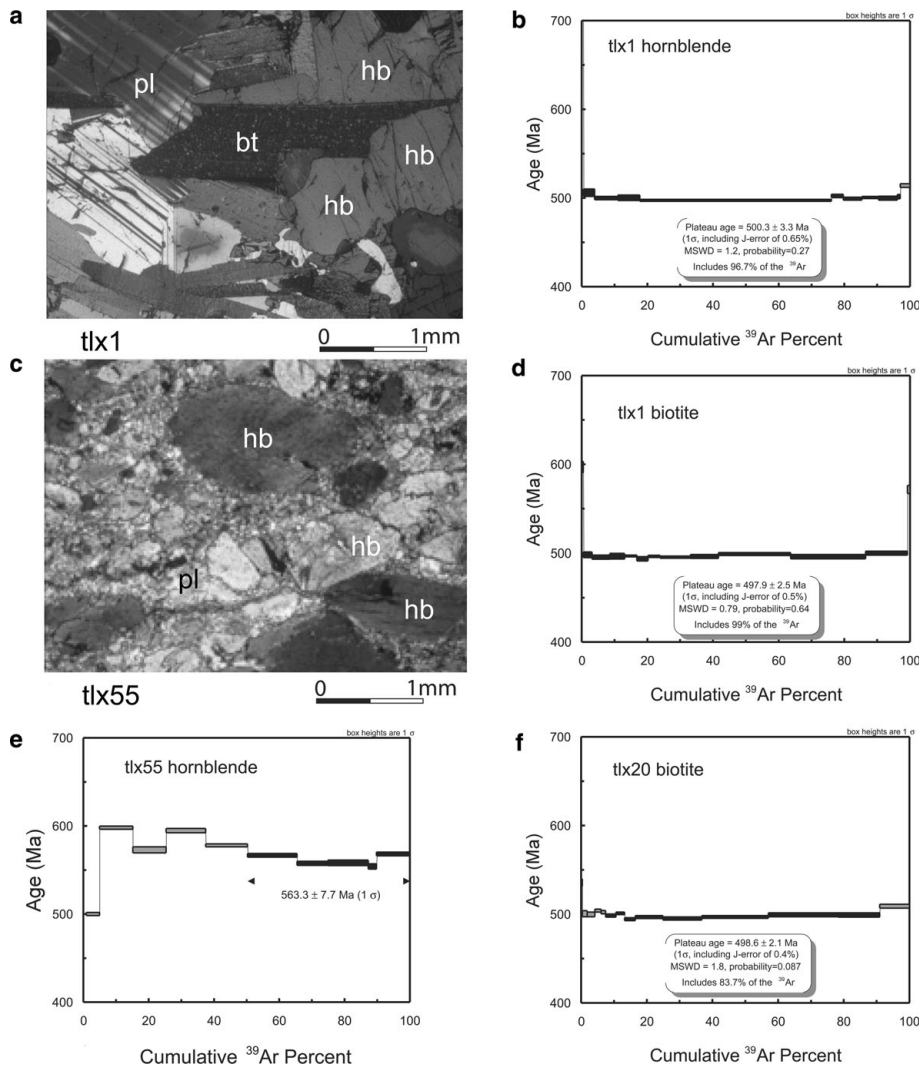
Fig. 4. Photomicrographs and associated hornblende (samples tlx1 and tlx55) and biotite (samples tlx1 and tlx20) ^{40}Ar/^{39}Ar spectra. Mineral abbreviations biotite (bt), hornblende (hb), plagioclase (pl). These ^{40}Ar/^{39}Ar step heating age spectra illustrate a *c.* 500 Ma event with an older ^{40}Ar/^{39}Ar plateau age of *c.* 560 Ma from hornblende in a matrix of fine recrystallized plagioclase within a mafic granulite.

continental collision (e.g. Fitzsimons 2000, 2003, Zhao *et al.* 2003), or 2) the "Kuunga" suture which is thought to pass through the southern Prince Charles Mountains (Boger *et al.* 2001, Boger & Miller 2004). The latter is believed to be associated with a collision between India and the East Antarctic shield. However, there is a dearth of geologic features, characteristic of collision orogens, which would support the latter interpretation (e.g. no obduction of ophiolite, no continental arc; Phillips *et al.* 2005). An alternative model proposed in this paper, suggests that the early Palaeozoic deformation was intraplate and driven by the temporal juxtaposition of distant plate boundary forces.

^{40}Ar/^{39}Ar thermochronology

Previous thermochronology

^{40}Ar/^{39}Ar thermochronology in the Prydz Bay region is limited to the Larsemann Hills (Zhao *et al.* 1992, Fu *et al.* 1993, Tong *et al.* 1998) and has highlighted the prominence of rapid early Palaeozoic cooling (*c.* 550–500 Ma), with possible relics of a late Mesoproterterozoic (*c.* 1100–1000 Ma) deformation event (Tong *et al.* 2002). There is a range of plateau ages from 552 Ma (hornblende), 494–485 Ma (biotite) and *c.* 455 Ma (K–feldspar). These ages, in addition to apatite fission ages of *c.* 210 Ma (Zhao *et al.* 1997) provide constraints on the cooling history following high-grade metamorphism.

An age for the peak metamorphic conditions within the Mather Paragneiss in the Rauer Group has been inferred to be 511 ± 4 Ma from *in situ* monazite chemical geochronology (Kelsey *et al.* 2003a). Recent work (Kelsey *et al.* 2007) recognizes two distinct age populations across the Prydz Bay region: early Palaeozoic (*c.* 570–520 Ma) and Neoproterozoic (*c.* 950–820 Ma), thus confirming the polymetamorphic nature of Prydz Bay. Intruded synchronously with the late stages of the early Palaeozoic deformation, in the Rauer Group, are planar pegmatite bodies that record SHRIMP U–Pb zircon ages of 518–507 Ma (Sims 1999).

Using apatite fission track data Lisker *et al.* (2005, 2007) have shown that there is a significantly different post-orogenic thermal history for the temperature interval 110–60°C, in the Prydz Bay region. These authors identify two major episodes of denudation in the late Palaeozoic and in the Cretaceous (Lisker *et al.* 2005, 2007). This led to the formation of the adjacent Lambert Graben, and to the Cretaceous Gondwana break-up between Antarctica and India.

Samples

Six rocks were selected for ^{40}Ar/^{39}Ar thermochronology, with each sample representing a different rock type associated with the high-strain zones (Table I). Hornblende, biotite and plagioclase samples were extracted from a garnet-bearing mafic granulite (tlx1). A hornblende sample (tlx55) was obtained from a garnet-bearing mafic granulite deformed in a high-strain zone (Fig. 4). A leucosome (tlx20) from a coarse-grained sapphirine/orthopyroxene–K–feldspar metapelite with minor biotite yielded biotite and K–feldspar that belong to the peak metamorphic assemblage. Biotite samples were obtained from rocks tlx29 and tlx35-2, which are pink syn-tectonic (2–5 m wide) and grey-white orthogneisses, respectively from Filla Island. These rocks are composed of coarse-grained K–feldspar, plagioclase, quartz, with minor biotite. K–feldspar sample (tlx37) derives from a syn-tectonic orthogneiss from Slon Island.

Methodology

The hornblende, biotite and feldspar separates were prepared using standard crushing, sieving, desliming, electromagnetic and heavy liquid mineral separation techniques. Separates were then hand-picked to greater than 99% purity. Sample weights were recorded and separates were packed into aluminium foil containers along with four intercalated flux monitor standards of GA1550 biotite (Age = 98.8 ± 0.5 Ma, Renne *et al.* 1998) and K_2SO_4 salts to determine correction factors for K-produced ^{40}Ar. Correction factors for interfering reactions are: $(^{36}Ar/^{37}Ar)_{Ca} = 3.50$ $(\pm 0.02) \times 10^{-4}$, $(^{39}Ar/^{37}Ar)_{Ca} = 7.9$ $(\pm 0.5) \times 10^{-4}$ and $(^{40}Ar/^{39}Ar)_K = 0.035$ (± 0.005). Samples were irradiated for 390 hours in position X34 of the HIFAR reactor, Lucas Heights, New South Wales, Australia. The canister, which was lined with 0.2 mm Cd to absorb thermal neutrons, was inverted three times during the irradiation. Irradiated samples, flux monitors and atmospheric blanks were analysed on a VG3600 mass spectrometer at the School of Earth Sciences, The University of Melbourne, using a Daly detector. Liberated gas was purified by SAES Zr–Al getters. Mass discrimination was monitored using analyses of purified air aliquots from a Dorflinger pipette. Isotopic data was corrected for mass spectrometer backgrounds, mass discrimination and fluence gradients. Unless otherwise stated errors in the age calculations are presented as 1σ-uncertainties and exclude errors associated with the *J*-value and decay constants (Steiger & Jäger 1977). K/Ca ratios were calculated as follows: K/Ca = 1.90 × ^{39}Ar/^{37}Ar.

A summary of the ^{40}Ar/^{39}Ar age data is presented in Table I while the complete ^{40}Ar/^{39}Ar dataset listed in Appendix I. Weighted mean plateau ages are defined for samples where three or more successive steps have an age within 2σ error of the mean, which together comprise >50% of total ^{39}Ar released. Total fusion ages (or total gas ages) represent pooled ages from all heating steps and are equivalent to conventional K–Ar ages. Inverse isochron plots of the corrected isotopic data produced clusters of points towards the abscissa and poorly defined regression lines, as a result of low levels of atmospheric argon within the samples. Consequently, isochron diagrams are not shown.

^{40}Ar/^{39}Ar results
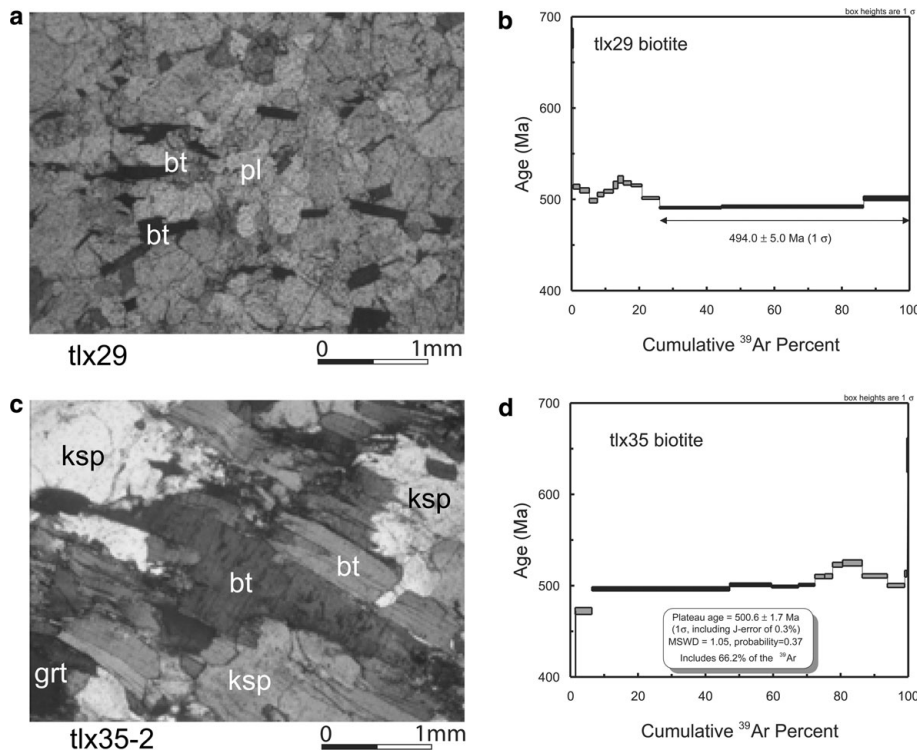
Hornblende

Hornblende from the garnet-bearing mafic granulite (Fig. 4a, sample tlx1) produced a flat age spectrum with a total fusion age of 505.1 ± 1.6 Ma (1σ). This is consistent with the weighted mean plateau age of 500.3 ± 3.3 Ma (1σ, including J-error), which includes 96.7% of ^{39}Ar gas released (Fig. 4b & Appendix I). The initial 0.44% and final heating steps of the age spectrum record elevated apparent ages, possibly due to release of minor amounts of excess argon from fluid/mineral inclusions.

Hornblende extracted from a sheared garnet-bearing mafic (Fig. 4c, sample tlx55) yielded a more discordant age spectrum with apparent ages generally decreasing with increasing temperature, for a total fusion age of 583.5 ± 2.4 Ma (1σ). A mean age of 563 ± 8 Ma (1σ, includes J-error) is calculated for the more concordant high temperature steps (Fig. 4e & Appendix A). The hornblende from this sample exhibits partial retrogression, suggesting that the discordance might be related to alteration-induced recoil redistribution/loss of ^{39}Ar and/or the incorporation of excess argon.

Biotite

A biotite separate from sample tlx1 (Fig. 4a) produced a concordant age spectrum with a total fusion age of 499.1 ± 2.0 Ma (1σ), compatible with the weighted mean plateau age of 497.9 ± 2.5 Ma (1σ, including J-error), which incorporates 99% of ^{39}Ar released (Fig. 4d & Appendix A). The lowest and highest temperature steps exhibit older apparent ages, but together represent only 1% of the ^{39}Ar

Fig. 5. Photomicrographs and associated biotite ^{40}Ar/^{39}Ar spectra (samples tlx29, and tlx35-2). Mineral abbreviations biotite (bt), garnet (grt), hornblende (hb), K-feldspar (ksp) and plagioclase (pl). The ^{40}Ar/^{39}Ar step heating age spectra of the biotites illustrate a *c.* 500 Ma event.

released. The plateau age is considered to represent the timing of cooling through the closure temperature for argon diffusion in biotite (~300°C; e.g. McDougall & Harrison 1999).

Biotite from a sapphirine-bearing leucosome (Fig. 4f, sample tlx20) in the Mather paragneiss yielded a flat age spectrum with a total fusion age of 500.0 ± 1.9 Ma (1σ) and a weighted mean plateau age of 498.6 ± 2.1 Ma $(1\sigma,$ including J-error), which includes 87.3% of ^{39}Ar released. The latter age is considered to reflect the time of biotite cooling through ~300 C.

Biotite from sample tlx29 (Fig. 5a) produced a somewhat discordant age spectrum with a total fusion age of 502.5 ± 3.1 Ma (1σ) (Fig. 5b). The discordance may be due to chlorite alteration (e.g. Di Vincenzo *et al.* 2003). The highest temperature steps give an average age of 494 ± 5 Ma $(1\sigma,$ including J-error), which is considered to represent a reasonable estimate for the time of biotite cooling below ~300°C. Biotite from Sample tlx35-2 (Fig. 5c) also yielded a slightly discordant age spectrum with a total fusion age of 499.2 ± 2.4 Ma (1σ) (Fig. 5d). However, intermediate temperature steps define an age plateau, with a weighted mean age of 500.6 ± 1.7 Ma for 66.2% of the total ^{39}Ar (Fig. 5d). The low temperature younger apparent ages are attributed to minor argon loss, with the higher temperature discordance suggestive of minor chlorite (?) alteration.

Feldspar

Plagioclase from sample tlx1 (Fig. 4a) yielded a disturbed age spectrum with a total fusion age of 512.4 ± 5.5 Ma.

With the exception of the lowest temperature step, apparent ages generally increase with increasing temperature from ~460 Ma to ~600 Ma (Fig. 6a & Appendix A). The more concordant, lower temperature, steps have an average age of 464 ± 3 Ma $(1\sigma,$ including J-error). The weighted mean plateau age is 482.3 ± 9.7 Ma, with ~72% of ^{39}Ar gas released. The increase in apparent ages shows a broad correlation with decreasing Ca/K ratios (Appendix A), suggesting possible contamination by an older, potassium-rich inclusion phase. However, co-existing biotite and hornblende both give younger plateau ages close to 500 Ma. Given the very low potassium contents of the plagioclase grains (<0.2 wt%K), it is possible that the older apparent ages are due to release of extraneous argon from fluid inclusions. If correct, then the average age of ~464 Ma may represent the best estimate for the time of plagioclase cooling below its argon closure temperature of ~250°C (e.g. McDougall & Harrison 1999).

K–feldspar from sample tlx20 (Fig 6b) produced an age spectrum showing apparent ages generally increasing (from a minimum age of 370.8 ± 4.0 Ma) with increasing temperature, for a total fusion age of 490.2 ± 11.1 Ma. The higher temperature steps give a weighted mean plateau age of 477.3 ± 3.7 Ma $(1\sigma,$ including J-error), which includes 75% of ^{39}Ar released. Interpretation of the age spectrum in terms of the multi-diffusion domain model (e.g. Lovera *et al.* 1997) would imply rapid cooling of coarser K–feldspar domains below their closure temperature of *c.* 300°C, followed by slower cooling for smaller domains through *c.* 200°C by *c.* 370 Ma (Fig. 6) K–feldspar from
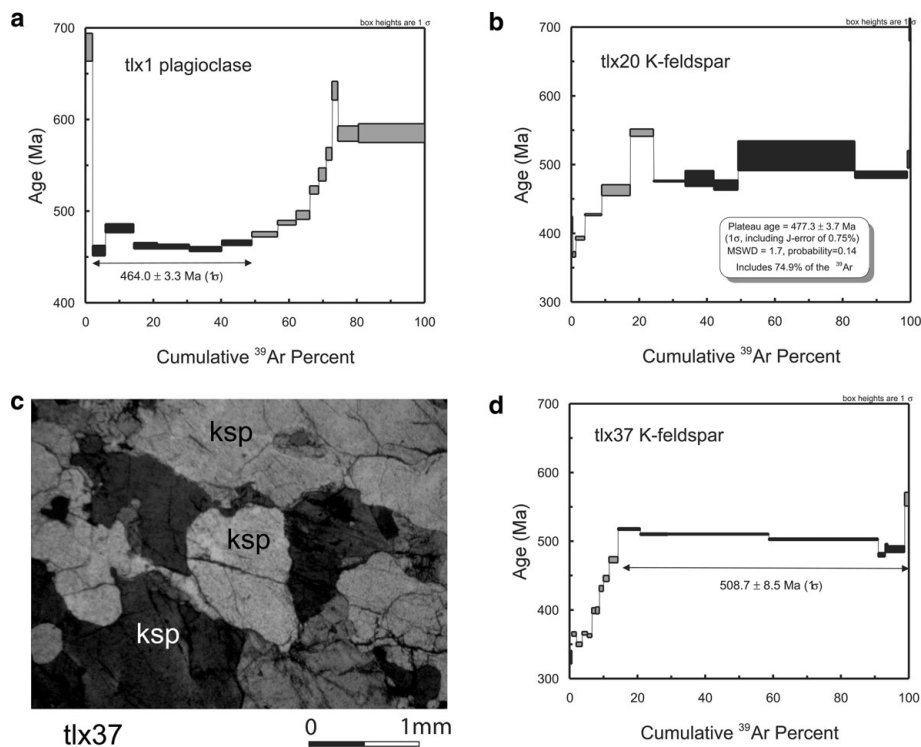
Fig. 6. ^{40}Ar/^{39}Ar step heating age spectra. **a.** plagioclase (sample tlx1), **b.** & **d.** K–feldspar (samples tlx20 and tlx37) and **c.** microstructure of the K-feldspar in tlx37.

sample tlx37 yielded broadly similar age spectrum with a total fusion age of 495.4 ± 2.1 Ma (Fig. 6a). No plateau age can be calculated for this sample, although the more concordant mid- to high-temperature steps have an average age of 508.7 ± 8.5 Ma (Fig. 6d & Appendix A). As above, this pattern may indicate relatively rapid cooling through the K–feldspar closure temperature of *c.* 300°C at *c.* 500 Ma for coarser domains, followed by slower cooling below *c.* 200°C by *c.* 370 Ma.

Discussion

Cooling history in the Rauer Group

The current study represents the first attempt to use ^{40}Ar/^{39}Ar thermochronology to constrain the post-orogenic cooling history in the Rauer Group during the early Palaeozoic. The well-defined ^{40}Ar/^{39}Ar plateau ages of *c.* 500 Ma for the hornblende in the mafic granulite (sample tlx1, Fig. 4b), suggests rapid cooling below the hornblende closure temperature of *c.* 500°C (e.g. McDougall & Harrison 1999) and is supported by a younger apparent age from co-existing biotite of *c.* 498 Ma (Fig. 4d); with the biotite closure temperature of *c.* 300°C. Similarly the co-existing plagioclase (Fig. 6a) may have a younger closure age of *c.* 460 Ma indicating the time when this mafic granulite cooled below its closure temperature of *c.* 200°C (e.g. McDougall & Harrison 1999). This rapid cooling is also indicated by the near-identical cooling ages

of *c.* 499 Ma derived from the other biotite samples (tlx20, tlx29, tlx35-2).

The apparently older cooling age (*c.* 560 Ma) and disturbed spectrum from the hornblende in sample tlx55 (Fig. 4e) may be a consequence of ^{40}Ar redistribution during the geologic evolution of these highly strained rocks, resulting in mixed ages and/or the presence of extraneous argon. Alternatively, comminution during shearing may have reduced grain domains, to the point where ^{39}Ar recoil loss/redistribution of ^{39}Ar becomes significant, thus producing older apparent ages from lower temperature heating steps.

Based on the data presented by Zhao *et al.* (1997) there is good reason to suspect that the cooling history of the Rauer Group might be representative of other areas in Prydz Bay and could reflect protracted residence of this crustal region throughout the early Palaeozoic. This was followed by a rapid regional cooling, with final cooling below 105–125°C occurring with a major denudation episode during the Permo–Carboniferous (Lisker *et al.* 2005).

Cooling rates

It is well recognized that the Rauer Group has experienced high-strain granulite-facies events in excess of 800°C (Harley & Fitzsimons 1995, Kelsey *et al.* 2003a, Tong & Wilson 2006) and that these are likely to be early Palaeozoic in age. The new ^{40}Ar/^{39}Ar age data of Rauer Group rocks compares reasonably well with existing *in situ* (Th + U)–Pb monazite age data (Kelsey *et al.* 2003b)
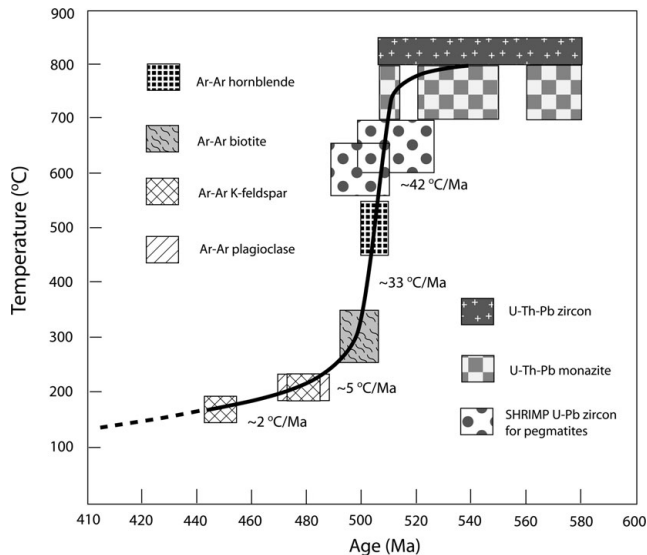
Fig. 7. Temperature-time path for the Rauer Group. Data boxes represent $^{40}Ar/^{39}Ar$ mineral ages, U–Th–Pb age data (Kelsey *et al.* 2003b) and SHRIMP U–Pb zircon ages (Kinny *et al.* 1993, Sims 1999). Box width indicates $\pm 2\sigma$ uncertainty limits for the age data. Box heights for $^{40}Ar/^{39}Ar$ data and U–Th–Pb zircon and monazite data are based on assumed closure temperatures. Box heights for syn-tectonic pegmatites represent estimates of regional temperatures during emplacement (600–700°C).

obtained from peak metamorphic assemblages. Namely, the cordierite-bearing symplectites (sapphirine + cordierite, orthopyroxene + corderite) that contain monazite age populations of *c.* 511 Ma (Kelsey *et al.* 2003b); the closure temperature of monazite is generally considered to be *c.* 700–750°C (Copeland *et al.* 1988, Parrish 1990, Smith & Giletti 1997), and even higher (*c.* 780°C) (Dahl 1997). Since the $^{40}Ar/^{39}Ar$ plateau age of *c.* 500 Ma recorded from hornblende in the garnet-bearing mafic granulite (Fig. 4b) indicates the time when the rock cooled below the hornblende closure temperature of *c.* 500°C, this reflects a high cooling rate of *c.* 40°C myr^{-1} from *c.* 510 Ma to *c.* 505 Ma. This is also consistent with that (*c.* 40°C myr^{-1}) reported by Zhao *et al.* (1997) for the Larsemann Hills. Similarly the $^{40}Ar/^{39}Ar$ plateau ages of *c.* 500 Ma obtained from the biotite samples (closure temperature of *c.* 300°C) further indicates a continued rapid cooling, with a cooling rate of *c.* 33°C myr^{-1} from *c.* 505 Ma to *c.* 500 Ma (Fig. 7).

Plagioclase generally has a closure temperature of 200–250°C in K–Ar system, whereas, K–feldspar has a closure temperature range of 150–300°C (McDougall & Harrison 1999). The similar $^{40}Ar/^{39}Ar$ ages of *c.* 465–480 Ma obtained from plagioclase (sample tlx1, Fig. 6a) and K–feldspar (sample tlx20, Fig. 6b) could suggest that they have similar closure temperatures (e.g. 200–250°C). If a closure temperature of *c.* 200°C is chosen for these

samples it would imply a cooling rate of *c.* 5°C myr^{-1} from *c.* 500 Ma to *c.* 480 Ma. Whereas, the $^{40}Ar/^{39}Ar$ plateau age of *c.* 480 Ma yielded from K–feldspar in a leucosome (sample tlx20, Fig. 6b) is younger than those recorded from samples tlx1 and tlx3. This suggests a lower blocking temperature than *c.* 200°C. If a closure temperature of *c.* 150°C is chosen, for sample tlx20, this would give a cooling rate of *c.* 2°C myr^{-1} from *c.* 480 Ma to *c.* 450 Ma.

Implications for Gondwana assembly

Any model for the tectonic evolution of the Rauer Group depends critically on the tectonic relationships assumed between its pre-Palaeozoic constituents prior to the commencement of an early Palaeozoic tectonothermal event. On the basis of relative structural correlations and geochemistry of mafic dykes, Sims *et al.* (1994) argued that the Vestfold Hills Block was juxtaposed with the Rauer Group at about 1000 Ma. Similarly, it is argued, on the basis of stratigraphic and geochronological evidence from the southern Prince Charles Mountains, that the Rauer Group and the Rayner Complex were all amalgamated before the early Palaeozoic events (Phillips *et al.* 2006). The correlation of Proterozoic ages between eastern India and east Antarctica (Crowe *et al.* 2001, Phillips *et al.* 2006) support the idea that much of east Gondwana was already comprised of East Antarctica, India and Australia as part of the Mawson continent by ~1000 Ma. In the Prydz Bay region this Rodinian supercontinent underwent a period of Neoproterozoic high-grade deformation and granite emplacement that has been interpreted as representing a collisional tectonic event (Fitzsimons 2000). There is also a Neoproterozoic rift basin in the southern Prince Charles Mountains that contains the Sodruzhestov series (Phillips *et al.* 2005) that was also deformed in the early Palaeozoic. Therefore, intraplate continental rifting within the region could provide a mechanism for the crustal deformation and an elevated geotherm during the late Neoproterozoic. These elevated thermal conditions would be the catalyst for the localization of the early Palaeozoic deformation in the high-strain zones seen in Prydz Bay and the pervasive early Palaeozoic deformation seen in the southern Prince Charles Mountains driven by passive stress fields generated from far off collisional orogens (Squire *et al.* 2006). This model does not require an early Palaeozoic "Kuunga suture" to explain the deformation in Prydz Bay and the Prince Charles Mountains, as proposed by Boger *et al.* (2001), Boger & Miller (2004).

Available palaeomagnetic data have been used (Meert 2003, Collins & Pisarevsky 2005) to suggest large horizontal movements between an Indo-Mawson continent and Africa occurred between *c.* 570–530 Ma. The initial collision of the Indian segment of east Gondwana with
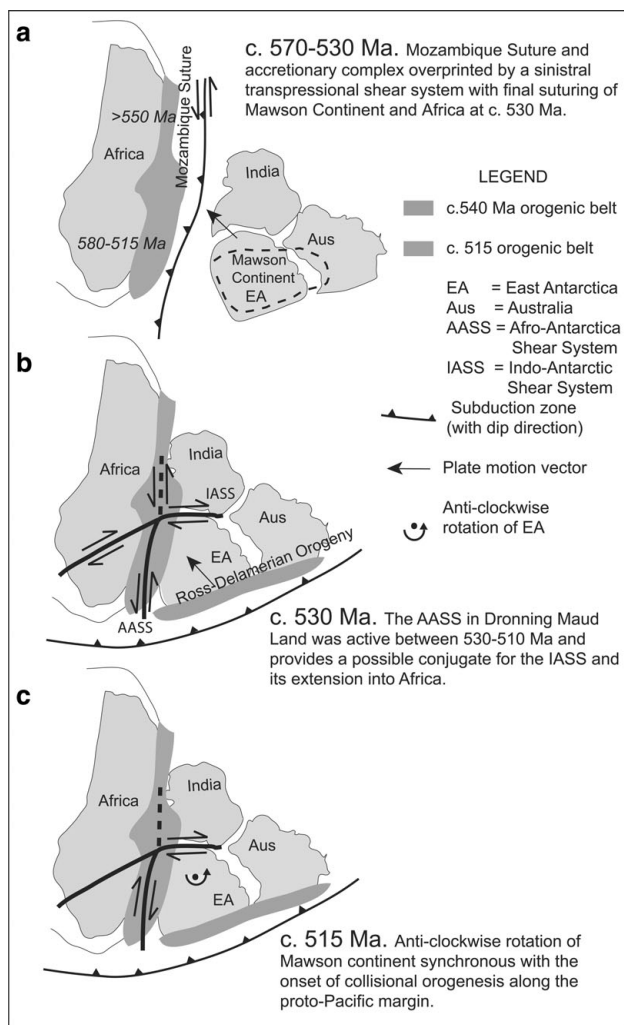
Fig. 8. Simplified model for Gondwana assembly and intracratonic deformation with the far-field stresses being associated with the initiation of active collisional orogenesis along the proto-Pacific margin. **a.** Intracratonic shear systems throughout Gondwana at *c.* 570–530 Ma (Meert 2003, Collins & Pisarevsky 2005.) may have initially developed in response to differential movement between India and the western margin of the Mawson Continent that can be implied from protracted and diachronous collision along the Mozambique Suture and associated accretionary complex. **b.** Initiation of convergence along the proto-Pacific margin (*c.* 530–520 Ma) induced north-west directed compression across Gondwana and induced a system of intracratonic shear zones, with the Afro-Antarctica shear system (AASS) in Dronning Maud Land (Jacobs *et al.* 2003) and the Indo-Antarctic (IASS) extending into Prydz Bay. **c.** Accretion on the proto-Pacific margin in south-eastern Australia accompanied by a passive margin environment along the margin to the west induced a rotational and extensional stress-field across Gondwana. This stress-field reversal is manifest in re-activation of the conjugate shear system with an overall anti-clockwise rotation.

west Gondwana (Fig. 8a at *c.* 550 Ma) would have induced a velocity differential such that the magnitude of the westerly-directed component diminished to the south. Thus the Mozambique suture between east and west Gondwana was diachronous with younger deformation to the south as described by Meert (2003). Following the suture of east and west Gondwana, north-westerly directed stresses induced by the initiation of convergence along the proto-Pacific margin (Fig. 8b at *c.* 530 Ma) caused a distal intraplate system of conjugate shears to develop, such as those seen in the Rauer Group (Fig. 3a). Differential movement along the proto-Pacific margin resulted in anti-clockwise rotation of the Mawson Continent with respect to Gondwana (Fig. 8c). This model does explain the rotation that is manifest in dextral reactivation of the Afro-Antarctic shear system (IASS) in Dronning Maud Land (Jacobs *et al.* 2003) that was synchronous with continued dextral movement in the Indo-Antarctic shear system in Prydz Bay (Carson *et al.* 1995). The Indo-Antarctic shear system is an extension of a series of large intracratonic transcurrent shear zones with sinistral displacement in Africa (Jacobs *et al.* 2003, Perritt & Watkeys 2003). The timing of the intra-cratonic shear system with northward tectonic escape and anti-clockwise rotation of the Mawson Continent corresponds with a shift from passive margin or continental arc tectonism to convergent orogenesis along the proto-Pacific margin of Gondwana (Boger & Miller 2004).

In Prydz Bay, this deformation was portioned and accommodated by a system of large-scale dextral shear zones that were active during the early Palaeozoic. The onset of shear localization, based on hornblende ages of *c.* 500 Ma, coincides well with the initiation of the thermal history of 511 Ma recorded in monazite data from the Rauer Group by Kelsey *et al.* (2003b). Episodic reactivation of the shear system continued in response to the evolving proto-Pacific margin from 530–420 Ma. However, there was no significant change in the macroscopic orientation of plate-motion vectors during this early Palaeozoic evolution (Fig. 8c).

Conclusions

The *c.* 550–500 Ma high-grade event in the Rauer Group is attributed to an intracratonic deformation regime where the high-strain zones are a response to distal plate boundary forces and plate-reorientation on the proto-Pacific margin. Then the far field stresses associated with north-west directed collision would induce the conjugate shear geometry preserved throughout east Antarctica, but the actual extent of this deformation is still unclear. However, the coincidence in ages between the major shear zones suggests a kinematic linkage exists across Gondwana. Thermochronological and metamorphic constraints from the Rauer Group indicate the occurrence of an elevated

thermal gradient during the late Neoproterozoic and a rapid cooling in the Early Palaeozoic. (c. 510–500 Ma) followed by a slow regional cooling from c. 500 Ma to c. 460 Ma.

The Prydz Bay region therefore represents a complex transpresssion zone, involving a significant component of transcurrent flow where recorded pressures (6–11 kbar, e.g. Fitzsimons & Harley 1997, Carson et al. 1995, Harley 1998, Kelsey et al. 2003a) suggest that overly thickened continental crust during high-temperature metamorphism is not required. There was also a pressure decrease (from c. 10 to 7 kbar, Kelsey et al. 2003a) during the cooling event that implies that post-orogenic collapse was a significant component during the late stage movement on these shear zones. Hence the responsiveness of the east Antarctic lithosphere during the early Palaeozoic was triggered by elevated thermal conditions that would provide the thermal induced weakening during an intraplate orogeny.

Acknowledgements

References

BOGER, S.D. & MILLER, J.M. 2004. Terminal suturing of Gondwana and the onset of the Ross-Delamerian Orogeny: the cause and effect of an Early Cambrian reconfiguration of plate motions. *Earth and Planetary Science Letters*, **219**, 511–527.

BOGER, S.D. & WILSON, C.J.L. 2005. Early Cambrian crustal shortening and a clockwise P-T-t path from the southern Prince Charles Mountains, East Antarctica: implications for the formation of Gondwana. *Journal of Metamorphic Geology*, **23**, 603–623.

BOGER, S.D., WILSON, C.J.L. & FANNING, C.M. 2001. Early Palaeozoic tectonism within the East Antarctic craton: the final suture between east and west Gondwana? *Geology*, **29**, 463–466.

BOGER, S.D., CARSON, C.J., WILSON, C.J.L. & FANNING, C.M. 2000. Neoproterozoic deformation in the Radok Lake region of the northern Prince Charles Mountains, east Antarctica: evidence for a single protracted orogenic event. *Precambrian Research*, **104**, 1–24.

BOGER, S.D., CARSON, C.J., FANNING, C.M., HERGT, J.M., WILSON, C.J.L. & WOODHEAD, J.D. 2002. Pan-African intraplate deformation in the northern Prince Charles Mountains, east Antarctica. *Earth and Planetary Science Letters*, **195**, 195–210.

CARSON, C.J., BOGER, S.D., FANNING, C.M., WILSON, C.J.L. & THOST, D.E. 2000. SHRIMP U–Pb geochronology from Mount Kirby, northern Prince Charles Mountains, East Antarctica. *Antarctic Science*, **12**, 429–442.

CARSON, C.J., DIRKS, P.H.G.M., HAND, M., SIMS, J.P. & WILSON, C.J.L. 1995. Compressional and extensional tectonics in low-medium pressure granulite from the Larsemann Hills, East Antarctica. *Geological Magazine*, **132**, 151–170.

CARSON, C.J., FANNING, C.M. & WILSON, C.J.L. 1996. Timing of the Progress Granite, Larsemann Hills: evidence for Early Palaeozoic orogenesis within the east Antarctic Shield and implications for Gondwana assembly. *Australian Journal of Earth Sciences*, **43**, 539–553.

COLLINS, A.S. & PISAREVSKY, S.A. 2005. Amalgamating eastern Gondwana: The evolution of the Circum-Indian Orogens. *Earth Science Reviews*, **71**, 229–270.

COPELAND, P., PARRISH, R.R. & HARRISON, T.M. 1988. Identification of inherited Pb in monazite and its implication for U–Pb systematic. *Nature*, **333**, 760–763.

CROWE, W.A., COSCA, M.A. & HARIS, L.B. 2001. ^{40}Ar–^{39}Ar geochronology and Neoproterozoic tectonics along the northern margin of the Eastern Ghats Belt in north Orissa, India. *Precambrian Research*, **108**, 237–266.

DAHL, P.S. 1997. A crystal-chemical basis for Pb retention and fission track annealing systematics in U-bearing minerals, with implications for geochronology. *Earth Planetary and Science Letters*, **150**, 277–290.

DIRKS, P.H.G.M., HOEK, J.D., WILSON, C.J.L. & SIMS, J.P. 1994. The Proterozoic deformation of the Vestfold Hills basement complex, east Antarctica: implications for the tectonic development of adjacent granulite belts. *Precambrian Research*, **65**, 277–295.

DIRKS, P.H.G.M. & HAND, M. 1995. Clarifying temperature-pressure paths via structures in granulite from the Bolingen Islands, Antarctica. *Australian Journal of Earth Sciences*, **42**, 157–172.

DIRKS, P.H.G.M. & WILSON, C.J.L. 1995. Crustal evolution of the east Antarctic mobile belt in Prydz Bay: continental collision at 500 Ma? *Precambrian Research*, **75**, 189–207

DI VINCENZO, G., VITI, C. & ROCCHO, S. 2003. The effect of chlorite interlayering on ^{40}Ar–^{39}Ar biotite dating: an ^{40}Ar–^{39}Ar laser-probe and TEM investigation of variably chloritised biotites. *Contributions to Mineralogy and Petrology*, **145**, 643–658.

FANNING, C.M., MOORE, D.H., BENNETT, V.C. & DALY, S.J. 1996. The "Mawson Continent": Archaean to Proterozoic crust in East Antarctica and the Gawler craton, Australia. A cornerstone in Rodinia and Gondwana. *Geological Society of Australia Abstracts*, **46**, 135.

FITZSIMONS, I.C.W. 1997. The Brattstrand paragneiss and the Sostrene orthogneiss: a review of Pan-African metamorphism and Grenvilian relics in southern Prydz Bay. *In* RICCI, C.A., ed. *The Antarctic region: geological evolution and processes*. Siena: Terra Antarctica, 121–130.

FITZSIMONS, I.C.W. 2000. Grenville-age basement provinces in East Antarctica: evidence from three separate collisional orogens. *Geology*, **28**, 879–882.

FITZSIMONS, I.C.W. 2003. Proterozoic basement provinces of southern and southwestern Australia, and their correlation with Antarctica. *In* YOSHIDA, M., WINDLEY, B.F. & DASGUPTA, S., eds. *Proterozoic East Gondwana: supercontinent assembly and breakup. Geological Society, London, Special Publications*, **206**, 93–130.

FITZSIMONS, I.C.W. & THOST, D.E. 1992. Geological relationships in high-grade basement gneiss of the northern Prince Charles Mountains, East Antarctica. *Australian Journal of Earth Sciences*, **39**, 173–193.

FITZSIMONS, I.C.W., KINNY, P.D. & HARLEY, S.L. 1997. Two stages of zircon and monazite growth in anatectic leucogneiss: SHRIMP constraints on the duration and intensity of Pan-African metamorphism in Prydz Bay, East Antarctica. *Terra Nova*, **9**, 47–51.

FU, Y., ZHAO, Y., WANG, Y., LIU, X. & LI, J. 1993. ^{40}Ar/^{39}Ar isotopic dating the biotites from the igneous and metamorphic rocks of the Zhongshan station area. *Antarctic Research*, **4**, 26–34.

GOLYNSKY, A.V., ALYAVDIN, S.V., MASOLOV, V.N., TSCHERINOV, A.S. & VOLNUKHIN, V.S. 2002. The composite magnetic anomaly map of the East Antarctic. *Tectonophysics*, **347**, 109–120.

HARLEY, S.L. 1997. Precambrian geological relationships in high-grade gneisses of the Rauer Islands, East Antarctica. *Australian Journal of Earth Sciences*, **34**, 175–207.

HARLEY, S.L. 1998. Ultrahigh temperature granulite metamorphism (1050°C, 12 kbar) and decompression in garnet (Mg70)-orthopyroxene-sillimanite gneisses from the Rauer Group, East Antarctica. *Journal of Metamorphic Geology*, **16**, 541–562.

HARLEY, S.L. & FITZSIMONS, I.C.W. 1991. Pressure-temperature evolution of metapelitic granulites in a polymetamorphic terrane: the Rauer Group, east Antarctica. *Journal of Metamorphic Geology*, **9**, 231–243.

HARLEY, S.L. & FITZSIMONS, I.C.W. 1995. High grade metamorphism and deformation in the Prydz Bay region, East Antarctica: terranes, events and regional correlations. *Journal of Geological Society of India*, **34**, 73–100.

HARLEY, S.L., SNAPE, I. & FITZSIMONS, I.C.W. 1995. Regional correlations and terrane assembly in East Prydz Bay: evidence from the Rauer Group and Vestfold Hills. *Terra Antartica*, **1**, 49–60.

HENSEN, B.J. & ZHOU, B. 1995. A Pan-African granulite facies metamorphic episode in Prydz Bay, Antarctica: evidence from Sm–Nd garnet dating. *Australian Journal of Earth Sciences*, **42**, 249–258.

JACOBS, J., KLEMD, R., FANNING, C.M., BAUER, W. & COLOMBO, F. 2003. Extensional collapse of the late Neoproterozoic–early Palaeozoic East African-Antarctic Orogen in central Drönning Maud Land, East Antarctica In YOSHIDA, M., WINDLEY, B.F. & DASGUPTA, S., eds. *Proterozoic East Gondwana: supercontinent assembly and breakup. Geological Society London, Special Publications*, **206**, 271–287.

JIANG, D. & WILLIAMS, P.F. 1998. High-strain zones: a unified model. *Journal of Structural Geology*, **20**, 1105–1120.

JIANG, D., LIN, S. & WILLIAMS, P.F. 2001. A fundamental problem with the kinematic interpretation of geological structures. *Journal of Structural Geology*, **21**, 933–937.

KELSEY, D.E., WHITE, R.W., POWELL, R., WILSON, C.J.L. & QUINN, C.D. 2003a. New constraints on metamorphism in the Rauer Group, Prydz Bay, east Antarctica. *Journal of Metamorphic Geology*, **21**, 739–759.

KELSEY, D.E., POWELL, R., WILSON, C.J.L. & STEELE, D.A. 2003b. (Th + U)–Pb monazite ages from Al–Mg-rich metapelites, Rauer Group, east Antarctica. *Contributions to Mineralogy and Petrology*, **126**, 326–340.

KELSEY, D.E., HAND, M., CLARK, C. & WILSON, C.J.L. 2007. On the application of *in situ* monazite chemical geochronology to constrain *P-T-t* histories in high temperature (>850°C) polymetamorphic granulites from Prydz Bay, east Antarctica. *Journal of the Geological Society London*, **164**, 667–683.

KINNY, P.D., BLACK, L.P. & SHERATON, J.W. 1993. Zircon ages and the distribution of Archaean and Proterozoic rocks in the Rauer Islands. *Antarctic Science*, **5**, 193–206.

KINNY, P.D., BLACK, L.P. & SHERATON, J.W. 1997. Zircon U–Pb ages and geochemistry of igneous and metamorphic rocks in the northern Prince Charles Mountains, Antarctica. *AGSO Journal of Australian Geology and Geophysics*, **16**, 637–654.

LISKER, F., BELTON, D.X & KRONER, U. 2005. Thermochronological investigations around the Lambert Graben: review of pre-existing data and field work during PCMEGA. *Terra Antarctica*, **12**, 45–50.

LISKER, F., WILSON, C.J.L. & GIBSON, H.J. 2007. Thermal history of the Vestfold Hills (East Antarctica) between Lambert rifting and Gondwana breakup; evidence from apatite fission track data. *Antarctic Science*, **19**, 97–106.

LIU, X., JAHN, B., ZHAO, Y., LI, M., LI, H. & LIU, X. 2006. Late Pan-African granitoids from the Grove Mountains, East Antarctica: age, origin and tectonic implications. *Precambrian Research*, **145**, 131–154.

LOVERA, O.M., GROVE, M., HARRISON, T.M. & MAHON, K.I. 1997. Systematic analysis of K-feldspar ^{40}Ar/^{39}Ar step-heating results: I. Significance of activation energy determinations. *Geochemical Cosmochimica Acta*, **61**, 3171–3192.

MCDOUGALL, I. & HARRISON, T.M. 1999. *Geochronology and thermochronology by the ^{40}Ar/^{39}Ar method*. Oxford: Oxford University Press, 269 pp.

MEERT, J.G. 2003. A synopsis of events related to the assembly of eastern Gondwana. *Tectonophysics*, **362**, 1–40.

PARRISH, R.R. 1990. U–Pb dating of monazite and its application to geological problems. *Canadian Journal of Earth Sciences*, **27**, 1431–1450.

PERRITT, S.H. & WATKEYS, M.K. 2003. Implications of late Pan-African shearing in western Drönning Maud Land, Antarctica. *In* STORTI, F., HOLDSWORTH, R.E. & SALVANI, F., eds. *Intraplate strike-slip deformation belts. Geological Society London, Special Publications*, **210**, 135–143.

PHILLIPS, G., WILSON, C.J.L. & FITZSIMONS, I.C.W. 2005. Stratigraphy and structure of the southern Prince Charles Mountains. *Terra Antartica*, **12**, 68–86.

PHILLIPS, G., WILSON, C.J.L. CAMPBELL, I.H. & ALLEN, C.M. 2006. U–Th–Pb detrital geochronology from the southern Prince Charles Mountains, East Antarctica - defining the Archaean to Neoproterozoic Ruker Province. *Precambrian Research*, **148**, 292–306.

PHILLIPS, G., WILSON, C.J.L., PHILLIPS, D. & SZCZEPANSKI, S.K. 2007. Thermochronological ^{40}Ar/^{39}Ar evidence for Early Palaeozoic basin inversion within the southern Prince Charles Mountains, East Antarctica: Implications for East Gondwana. *Journal of the Geological Society London*, **145**, 771–784.

RENNE, P.R., SWISHER, C.C., DEINO, A.L., KARNER, D.B., OWENS, T.L. & DEPAOLO, D.J. 1998. Intercalibration of standards, absolute ages and uncertainties in ^{40}Ar/^{39}Ar dating. *Chemical Geology*, **145**, 117–152.

SIMS, J.P. 1999. *The structural and metamorphic evolution of a granulite-facies gneiss terrain: the Rauer Group, east Antarctica*. PhD thesis, The University of Melbourne, 205 pp. [Unpublished]

SIMS, J.P., DIRKS, P.H.G.M., CARSON, C.J. & WILSON, C.J.L. 1994. The structural evolution of the Rauer Group, east Antarctica: mafic dykes as passive markers in a composite Proterozoic terrain. *Antarctic Science*, **6**, 379–394.

SIMS, J.P. & WILSON, C.J.L. 1997. Strain localization and texture development in a granulite-facies shear zone - the Rauer Group, East Antarctica. *In* RICCI, C.A., ed. *The Antarctic Region: geological evolution and processes*. Siena: Terra Antartica, 131–138.

SMITH, H.A. & GILETTI, B.J. 1997. Pb diffusion in monazite. *Geochimica et Cosmochimica Acta*, **61**, 1047–1055.

SQUIRE, R.J., CAMPBELL, H.I., ALLEN, C.M. & WILSON, C.J.L. 2006. Did the Transgondwanan Supermountain trigger the explosive radiation of animals on Earth? *Earth and Planetary Sciences Letters*, **250**, 116–133.

STEIGER, R.H. & JÄGER, E. 1977. Subcommission on geochronology: convention on the use of decay constants in geo- and cosmochronology. *Earth and Planetary Science Letters*, **36**, 359–362.

TONG, L. & WILSON, C.J.L. 2006. Tectonothermal evolution of the ultrahigh temperature metapelites in the Rauer Group, east Antarctica. *Precambrian Research*, **149**, 1–20.

TONG, L., WILSON, C.J.L. & LIU, X. 2002. A high-grade event of ~1100 Ma preserved within the ~500 Ma mobile belt of the Larsemann Hills, east Antarctica: further evidence from ^{40}Ar–^{39}Ar dating. *Terra Antartica*, **9**, 73–86.

TONG, L., LIU, X., ZHANG, L., CHEN, H., CHEN, F., WANG, Y. & REN, L. 1998. The ^{40}Ar–^{39}Ar ages of hornblendes in Grt–Pl-bearing amphibolite from the Larsemann Hills, East Antarctica and their geological implications. *Chinese Journal of Polar Research*, **9**, 79–91.

ZIEMANN, M.A., FÖRSTER, H.-J., HARLOV, D.E. & FREI, D. 2005. Origin of fluorapatite-monazite assemblages in a metamorphosed, sillimanite-bearing pegmatoid, Reinbolt Hills, East Antarctica. *European Journal of Mineralogy*, **17**, 567–579.

ZHAO, Y., SONG, B., WANG, Y., REN, L., LI, J. & CHEN, T. 1992. Geochronology of the late granite in the Larsemann Hills, East Antarctica. *In* YOSHIDA, Y., KAMINUMA, K. & SHIRAISHI, K., eds. *Recent progress in Antarctic Earth Science*. Tokyo: Terra Scientific Publishing, 155–161.

ZHAO, Y., LIU, X., WANG, S. & SONG, B. 1997. Syn- and post-tectonic cooling and exhumation in the Larsemann Hills, East Antarctica. *Episodes*, **20**, 122–127.

ZHAO, Y., LIU, X.H., LIU, X.C. & SONG, B. 2003. Pan-African events in Prydz Bay, East Antarctica, and their implications for East Gondwana tectonics. *In* YOSHIDA, M., WINDLEY, B.F. & DASGUPTA, S., eds. *Proterozoic East Gondwana: supercontinent assembly and breakup. Geological Society London, Special Publications*, **206**, 231–245.

Appendix

Appendix A. ^{40}Ar/^{39}Ar step-heating analysis results for the Rauer Group.

T (°C)	^{36}Ar (mol)	^{37}Ar (mol)	^{39}Ar (mol)	^{40}Ar (mol)	^{40}Ar* (%)	^{40}Ar*/^{39}K	^{39}Ar (%)	Age (Ma) ± 1 SD	Ca/K
tlx1 hornblende: $J = 0.009722 \pm 0.651$									
800	7.85E-17	3.46E-15	1.03E-15	2.14E-13	89.3	186.35	0.24	1865.1 ± 13.5	6.40E + 00
900	1.23E-17	2.26E-15	8.57E-16	4.64E-14	92.7	50.25	0.44	717.6 ± 6.6	5.02E + 00
980	3.91E-17	4.28E-14	1.48E-14	5.01E-13	98.5	33.34	3.87	506.6 ± 4.2	5.50E + 00
1010	6.61E-17	8.77E-14	3.07E-14	1.02E-12	98.9	32.90	10.98	500.6 ± 1.8	5.45E + 00
1030	5.33E-17	8.50E-14	2.87E-14	9.51E-13	99.2	32.92	17.64	501.0 ± 3.0	5.64E + 00
1050	5.37E-16	7.39E-13	2.52E-13	8.32E-12	98.9	32.70	76.10	498.0 ± 1.1	5.58E + 00
1060	3.22E-17	4.44E-14	1.52E-14	5.07E-13	98.9	33.07	79.63	502.9 ± 1.8	5.56E + 00
1080	5.47E-17	7.32E-14	2.49E-14	8.26E-13	98.9	32.83	85.41	499.8 ± 1.6	5.59E + 00
1100	4.96E-17	6.28E-14	2.16E-14	7.19E-13	98.8	32.94	90.42	501.2 ± 1.3	5.53E + 00
1130	5.14E-17	7.43E-14	2.49E-14	8.26E-13	99.0	32.88	96.20	500.4 ± 2.2	5.68E + 00
1160	1.59E-17	1.21E-14	3.86E-15	1.31E-13	97.3	33.01	97.09	502.2 ± 2.4	5.97E + 00
1450	1.19E-16	3.66E-14	1.26E-14	4.57E-13	93.0	33.95	100.00	514.6 ± 2.0	5.56E + 00
Total	1.11E-15	1.26E-12	4.31E-13	1.45E-11		33.23		505.1 ± 1.6	
tlx1 biotite: $J = 0.00974 \pm 0.501$									
600	1.48E-20	2.42E-19	3.07E-16	1.24E-14	99.9	40.31	0.29	597.4 ± 6.2	1.50E-03
700	2.59E-17	9.06E-17	2.89E-15	1.02E-13	92.5	32.72	3.04	499.1 ± 3.0	5.96E-02
750	1.54E-17	7.88E-17	5.63E-15	1.88E-13	97.5	32.55	8.39	496.7 ± 2.5	2.66E-02
780	8.44E-18	1.23E-16	4.87E-15	1.62E-13	98.4	32.60	13.03	497.5 ± 3.0	4.80E-02
810	7.30E-18	7.79E-17	3.84E-15	1.28E-13	98.2	32.64	16.68	498.0 ± 1.1	3.85E-02
840	6.46E-18	2.47E-19	3.51E-15	1.16E-13	98.3	32.41	20.02	494.9 ± 2.3	1.34E-04
900	9.40E-18	4.31E-17	3.98E-15	1.33E-13	97.8	32.61	23.80	497.6 ± 1.2	2.06E-02
950	1.68E-17	9.84E-17	9.70E-15	3.21E-13	98.4	32.53	33.03	496.6 ± 1.2	1.93E-02
1000	1.11E-17	7.96E-19	8.97E-15	2.96E-13	98.8	32.60	41.56	497.4 ± 2.2	1.69E-04
1050	2.45E-17	1.65E-16	2.31E-14	7.65E-13	99.0	32.78	63.53	499.9 ± 1.5	1.36E-02
1100	6.80E-18	5.56E-17	2.41E-14	7.89E-13	99.7	32.59	86.48	497.3 ± 2.3	4.38E-03
1150	1.48E-18	1.70E-18	1.34E-14	4.42E-13	99.8	32.86	99.26	501.0 ± 1.9	2.41E-04
1350	6.01E-17	8.03E-17	7.77E-16	4.76E-14	62.6	38.32	100.00	572.2 ± 4.7	1.96E-01
Total	1.94E-16	8.16E-16	1.05E-13	3.50E-12		32.73		499.1 ± 2.0	
tlx1 plagioclase: $J = 0.00972 \pm 651$									
650	2.19E-17	2.49E-14	3.80E-16	2.08E-14	81.2	46.97	1.85	678.6 ± 15.2	1.31E + 02
725	2.20E-17	4.17E-14	7.87E-16	2.46E-14	91.1	29.73	5.72	458.0 ± 5.7	1.05E + 02
800	2.76E-17	7.97E-14	1.69E-15	5.11E-14	100	31.53	14.06	482.3 ± 4.8	9.33E + 01
850	2.37E-17	6.06E-14	1.41E-15	4.17E-14	98.2	30.12	21.03	463.4 ± 3.4	8.47E + 01
900	2.93E-17	7.68E-14	1.90E-15	5.60E-14	98.6	30.07	30.47	462.6 ± 2.5	7.94E + 01
950	2.68E-17	6.93E-14	1.93E-15	5.67E-14	98.6	29.86	40.07	459.8 ± 2.6	7.04E + 01
1000	2.37E-17	5.72E-14	1.77E-15	5.36E-14	97.9	30.35	48.94	466.5 ± 2.9	6.29E + 01
1050	1.71E-17	4.15E-14	1.53E-15	4.72E-14	98.3	31.04	56.61	475.8 ± 2.7	5.28E + 01
1100	1.47E-17	2.75E-14	1.08E-15	3.54E-14	95.7	31.98	62.06	488.5 ± 2.6	4.92E + 01
1150	1.42E-17	2.15E-14	8.05E-16	2.77E-14	92.8	32.60	66.10	496.7 ± 4.8	5.19E + 01
1200	1.42E-17	1.43E-14	5.16E-16	2.02E-14	86.6	34.66	68.69	523.9 ± 4.3	5.39E + 01
1250	1.52E-17	1.32E-14	4.36E-16	1.84E-14	83.0	35.94	70.88	540.6 ± 7.0	5.89E + 01
1300	1.79E-17	1.21E-14	3.60E-16	1.72E-14	76.6	37.67	72.68	563.0 ± 6.8	6.57E + 01
1350	2.19E-17	1.27E-14	3.47E-16	1.97E-14	73.8	43.11	74.40	631.4 ± 10.2	7.19E + 01
1400	5.46E-17	4.46E-14	1.21E-15	5.80E-14	80.1	39.40	80.46	585.1 ± 8.2	7.19E + 01
1450	2.24E-16	9.99E-14	3.89E-15	2.06E-13	72.8	39.44	100.00	585.5 ± 10.2	4.98E + 01
Total	5.69E-16	6.98E-13	2.00E-14	7.55E-13		33.78		512.4 ± 5.5	
tlx55 hornblende: $J = 0.00972 \pm 0.601$									
800	4.88E-17	8.69E-15	1.67E-15	3.10E-13	95.6	178.664	0.67	1816.5 ± 14.0	9.94E + 00
900	3.20E-17	8.58E-15	1.01E-14	3.40E-13	97.4	32.942	4.75	501.2 ± 1.8	1.62E + 00
980	8.49E-17	6.54E-14	2.53E-14	1.04E-12	98.2	40.482	14.97	598.7 ± 1.9	4.93E + 00
1010	7.20E-17	8.11E-14	2.54E-14	9.87E-13	98.6	38.505	25.22	573.7 ± 3.4	6.09E + 00
1040	8.84E-17	9.79E-14	2.98E-14	1.21E-12	98.6	40.214	37.26	595.4 ± 2.3	6.26E + 00
1060	9.25E-17	1.04E-13	3.19E-14	1.26E-12	98.6	38.907	50.17	578.8 ± 1.6	6.18E + 00
1080	9.45E-17	1.22E-13	3.75E-14	1.44E-12	98.9	38.012	65.33	567.4 ± 2.1	6.22E + 00
1100	7.09E-17	8.04E-14	2.36E-14	8.92E-13	98.5	37.302	74.87	558.3 ± 2.3	6.49E + 00

Continued

^{40}Ar* = radiogenic ^{40}Ar corrected for atmospheric ^{40}Ar, SD = standard deviation.

Appendix A. Continued

T (°C)	^{36}Ar (mol)	^{37}Ar (mol)	^{39}Ar (mol)	^{40}Ar (mol)	^{40}Ar* (%)	^{40}Ar*/^{39}K	^{39}Ar (%)	Age (Ma) ± 1 SD	Ca/K
1130	8.31E-17	1.07E-13	3.02E-14	1.14E-12	98.7	37.360	87.09	559.0 ± 3.3	6.72E + 00
1170	4.07E-17	2.42E-14	6.52E-15	2.50E-13	96.1	37.034	89.73	554.8 ± 3.0	7.08E + 00
1450	2.11E-16	8.84E-14	2.54E-14	1.02E-12	94.7	38.147	100.00	569.1 ± 2.1	6.63E + 00
Total	9.19E-16	7.87E-13	2.47E-13	9.89E-12		39.276		583.5 ± 2.4	
tlx20 biotite: J = 0.00974 ± 0.41									
600	3.06E-18	7.04E-18	1.47E-16	6.13E-15	85.2	35.55	0.13	536.4 ± 4.1	9.10E-02
700	5.74E-18	3.54E-18	1.84E-15	6.24E-14	97.2	32.90	1.74	501.4 ± 3.3	3.65E-03
750	8.05E-18	2.28E-19	2.52E-15	8.53E-14	97.1	32.84	3.95	500.7 ± 2.6	1.72E-04
780	7.04E-18	1.70E-17	2.16E-15	7.38E-14	97.1	33.16	5.84	504.9 ± 1.7	1.50E-02
810	5.20E-18	2.28E-19	1.65E-15	5.61E-14	97.2	33.03	7.28	503.2 ± 1.8	2.63E-04
840	9.57E-18	4.03E-18	3.70E-15	1.24E-13	97.6	32.75	10.52	499.4 ± 1.8	2.07E-03
870	4.81E-18	2.28E-19	2.96E-15	9.89E-14	98.5	32.94	13.11	502.0 ± 1.5	1.47E-04
900	7.89E-18	1.22E-17	3.68E-15	1.22E-13	98.0	32.44	16.33	495.3 ± 1.7	6.31E-03
950	9.97E-18	1.00E-16	9.69E-15	3.19E-13	99.0	32.62	24.81	497.8 ± 1.7	1.96E-02
1000	1.03E-17	4.96E-17	1.36E-14	4.46E-13	99.2	32.50	36.71	496.2 ± 1.8	6.92E-03
1050	1.22E-17	6.92E-17	2.32E-14	7.60E-13	99.4	32.64	56.97	497.9 ± 1.4	5.68E-03
1100	1.02E-19	2.14E-16	2.43E-14	8.00E-13	99.9	32.82	78.27	500.4 ± 2.1	1.67E-02
1150	1.52E-17	7.58E-17	1.45E-14	4.80E-13	99.0	32.79	90.96	500.0 ± 2.4	9.93E-03
1350	2.14E-16	7.36E-19	1.03E-14	4.10E-13	84.5	33.53	100.00	509.8 ± 2.1	1.35E-04
Total	3.13E-16	5.54E-16	1.14E-13	3.84E-12		32.79		500.0 ± 1.9	
tlx20 K-feldspar: J = 0.00977 ± 0.751									
600	5.40E-18	3.41E-18	2.76E-16	8.89E-15	82.0	26.46	0.21	414.9 ± 11.0	2.35E-02
700	2.33E-18	3.41E-18	1.20E-15	2.88E-14	97.5	23.35	1.12	370.8 ± 4.0	5.40E-03
800	6.68E-18	9.25E-16	3.57E-15	9.11E-14	97.8	25.01	3.82	394.4 ± 2.5	4.93E-01
900	9.23E-18	2.01E-15	6.56E-15	1.83E-13	98.5	27.41	8.80	428.2 ± 1.3	5.83E-01
1000	1.36E-17	2.85E-15	1.11E-14	3.37E-13	98.8	30.00	17.23	463.8 ± 7.9	4.87E-01
1050	3.50E-18	1.10E-17	9.07E-15	3.30E-13	99.6	36.24	24.10	547.0 ± 5.4	2.31E-03
1100	1.76E-17	4.29E-15	1.23E-14	3.85E-13	98.7	30.96	33.41	476.9 ± 1.1	6.64E-01
1150	1.74E-17	5.50E-15	1.13E-14	3.58E-13	98.6	31.25	41.98	480.9 ± 11.5	9.26E-01
1200	1.51E-17	3.60E-15	9.32E-15	2.89E-13	98.5	30.54	49.05	471.2 ± 7.3	7.33E-01
1250	2.18E-17	1.01E-14	4.55E-14	1.54E-12	99.6	33.70	83.55	513.6 ± 21.3	4.23E-01
1300	3.79E-17	8.73E-15	2.04E-14	6.55E-13	98.3	31.65	99.00	486.2 ± 5.1	8.14E-01
1350	2.61E-17	1.08E-15	8.92E-16	3.73E-14	79.6	33.31	99.68	508.4 ± 12.5	2.30E + 00
1400	1.01E-16	3.48E-18	4.27E-16	5.05E-14	40.7	48.17	100.00	695.9 ± 16.5	1.55E-02
Total	2.78E-16	3.91E-14	1.32E-13	4.29E-12		31.95		490.2 ± 11.1	
tlx29-2 biotite: J = 0.00976 ± 0.31									
600	8.23E-18	3.95E-17	1.48E-16	9.34E-15	74.0	46.63	0.24	676.4 ± 10.8	5.07E-01
700	7.41E-18	3.18E-17	1.24E-15	4.41E-14	95.0	33.84	2.24	514.7 ± 2.6	4.89E-02
750	7.05E-18	3.11E-17	1.74E-15	6.07E-14	96.5	33.56	5.06	510.9 ± 2.7	3.39E-02
780	6.62E-18	6.40E-17	1.53E-15	5.20E-14	96.2	32.70	7.53	499.5 ± 2.5	7.96E-02
810	5.66E-18	6.34E-17	1.13E-15	3.93E-14	95.7	33.21	9.36	506.3 ± 2.4	1.06E-01
840	7.95E-18	6.33E-17	1.71E-15	5.96E-14	96.0	33.46	12.13	509.7 ± 1.9	7.03E-02
870	4.19E-18	3.02E-17	9.26E-16	3.27E-14	96.2	33.99	13.62	516.7 ± 4.0	6.20E-02
900	4.97E-18	4.86E-17	9.41E-16	3.39E-14	95.6	34.45	15.15	522.7 ± 4.0	9.81E-02
950	6.81E-18	7.32E-17	1.43E-15	5.10E-14	96.0	34.15	17.46	518.7 ± 2.2	9.71E-02
1000	6.39E-18	6.21E-17	1.97E-15	6.89E-14	97.2	33.97	20.65	516.3 ± 1.5	5.98E-02
1050	8.30E-18	8.04E-17	3.25E-15	1.10E-13	97.7	32.92	25.91	502.5 ± 1.5	4.70E-02
1100	1.87E-17	2.47E-16	1.14E-14	3.71E-13	98.4	32.14	44.27	492.0 ± 1.2	4.14E-02
1150	4.00E-17	5.60E-16	2.60E-14	8.50E-13	98.5	32.21	86.34	493.0 ± 1.5	4.09E-02
1350	6.34E-17	2.35E-16	8.45E-15	2.97E-13	93.6	32.89	100.00	502.0 ± 2.4	5.28E-02
Total	1.96E-16	1.63E-15	6.18E-14	2.08E-12		32.66		499.0 ± 1.8	
tlx35-2 biotite: J = 0.00977 ± 0.31									
600	8.19E-18	2.19E-19	1.21E-15	1.98E-14	87.6	14.34	1.27	236.7 ± 3.8	3.45E-04
700	5.57E-17	3.03E-17	4.68E-15	1.60E-13	89.6	30.71	6.19	473.5 ± 3.7	1.23E-02
750	4.10E-17	2.19E-18	3.89E-14	1.28E-12	99.0	32.48	47.08	497.4 ± 2.3	1.07E-04
780	2.84E-18	1.05E-16	1.18E-14	3.87E-13	99.7	32.83	59.44	502.0 ± 2.0	1.70E-02
810	5.59E-18	4.52E-17	7.58E-15	2.50E-13	99.3	32.68	67.41	500.0 ± 1.5	1.13E-02

Continued

Appendix A. Continued

T (°C)	^{36}Ar (mol)	^{37}Ar (mol)	^{39}Ar (mol)	^{40}Ar (mol)	^{40}Ar* (%)	^{40}Ar*/^{39}K	^{39}Ar (%)	Age (Ma) ± 1 SD	Ca/K
840	5.69E-18	2.65E-17	4.68E-15	1.55E-13	98.8	32.82	72.34	501.8 ± 1.6	1.08E-02
870	4.56E-18	4.62E-17	2.80E-15	9.52E-14	98.5	33.51	75.28	511.0 ± 2.3	3.13E-02
900	6.04E-18	3.64E-17	2.17E-15	7.46E-14	97.5	33.53	77.56	511.3 ± 2.6	3.19E-02
950	9.29E-18	8.49E-17	2.84E-15	1.01E-13	97.2	34.46	80.55	523.7 ± 2.6	5.68E-02
1000	1.11E-17	5.35E-17	5.47E-15	1.93E-13	98.2	34.62	86.31	525.8 ± 3.2	1.86E-02
1050	1.25E-17	1.33E-16	7.11E-15	2.42E-13	98.4	33.55	93.79	511.6 ± 2.3	3.55E-02
1100	1.09E-17	4.59E-16	4.88E-15	1.63E-13	98.0	32.77	98.92	501.2 ± 2.1	1.79E-01
1150	1.31E-17	1.62E-16	6.96E-16	2.73E-14	85.8	33.74	99.65	514.1 ± 3.5	4.44E-01
1350	1.44E-16	9.88E-17	3.36E-16	5.72E-14	25.7	43.82	100	643.1 ± 18.8	5.59E-01
Total	3.30E-16	1.28E-15	9.51E-14	3.20E-12		32.62		499.2 ± 2.4	
tlx37 K-feldspar: $J = 0.00976 ± 0.71$									
500	1.48E-20	3.15E-18	1.65E-16	1.69E-14	99.9	102.20	0.18	1247.9 ± 7.9	3.63E-02
575	4.06E-18	6.65E-16	2.39E-16	6.09E-15	81.3	20.78	0.45	333.0 ± 9.9	5.31E + 00
650	4.37E-18	9.46E-17	1.24E-15	3.00E-14	95.6	23.10	1.82	366.6 ± 3.1	1.45E-01
700	3.65E-18	3.15E-18	1.49E-15	3.41E-14	96.7	22.06	3.47	351.7 ± 3.3	4.01E-03
750	5.29E-18	1.08E-15	1.49E-15	3.59E-14	95.8	23.17	5.12	367.7 ± 2.4	1.38E + 00
800	6.27E-18	1.66E-15	1.16E-15	2.83E-14	94.0	22.94	6.40	364.4 ± 2.5	2.71E + 00
850	1.46E-18	7.57E-16	9.97E-16	2.57E-14	98.5	25.46	7.50	400.2 ± 4.3	1.44E + 00
900	4.33E-18	1.39E-15	9.70E-16	2.59E-14	95.5	25.50	8.58	400.8 ± 5.0	2.73E + 00
950	2.21E-18	3.46E-16	1.11E-15	3.13E-14	97.9	27.75	9.80	432.3 ± 4.2	5.95E-01
1000	7.23E-18	1.14E-15	1.50E-15	4.53E-14	95.5	28.82	11.46	447.0 ± 4.4	1.45E + 00
1050	1.49E-17	1.31E-15	2.38E-15	7.77E-14	94.4	30.83	14.09	474.3 ± 4.4	1.05E + 00
1100	2.04E-17	2.50E-15	5.95E-15	2.09E-13	97.2	34.13	20.68	518.5 ± 1.7	7.97E-01
1150	1.28E-17	7.28E-18	7.29E-15	2.49E-13	98.4	33.56	28.75	510.9 ± 1.5	1.90E-03
1200	4.89E-17	7.11E-15	2.70E-14	9.21E-13	98.4	33.57	58.65	511.0 ± 1.1	5.00E-01
1250	1.51E-17	2.23E-17	2.91E-14	9.67E-13	99.5	33.03	90.90	503.9 ± 1.6	1.45E-03
1300	1.32E-17	2.17E-15	1.96E-15	6.52E-14	94.3	31.32	93.07	481.0 ± 3.0	2.10E + 00
1350	1.69E-17	1.18E-15	6.72E-16	2.64E-14	81.5	32.06	93.82	491.0 ± 6.4	3.35E + 00
1450	3.51E-17	1.66E-15	4.41E-15	1.51E-13	93.2	31.94	98.70	489.3 ± 4.8	7.17E-01
1500	1.03E-16	3.35E-18	1.18E-15	7.45E-14	59.3	37.43	100.00	561.5 ± 9.8	5.39E-03
Total	3.19E-16	2.31E-14	9.04E-14	3.02E-12		32.39		495.4 ± 2.1	

^{40}Ar* = radiogenic ^{40}Ar corrected for atmospheric ^{40}Ar, SD = standard deviation.